JCI The Journal of Clinical Investigation

Combined MEK and JAK inhibition abrogates murine myeloproliferative neoplasm

Guangyao Kong, … , James C. Mulloy, Jing Zhang

J Clin Invest. 2014;124(6):2762-2773. https://doi.org/10.1172/JCI74182.

Research Article **Hematology**

Overactive RAS signaling is prevalent in juvenile myelomonocytic leukemia (JMML) and the myeloproliferative variant of chronic myelomonocytic leukemia (MP-CMML) in humans, and both are refractory to conventional chemotherapy. Conditional activation of a constitutively active oncogenic *Nras* ($Nras^{G12D/G12D}$) in murine hematopoietic cells promotes an acute myeloproliferative neoplasm (MPN) that recapitulates many features of JMML and MP-CMML. We found that $Nras^{G12D/G12D}$-expressing HSCs, which serve as JMML/MP-CMML–initiating cells, show strong hyperactivation of ERK1/2, promoting hyperproliferation and depletion of HSCs and expansion of downstream progenitors. Inhibition of the MEK pathway alone prolonged the presence of $Nras^{G12D/G12D}$-expressing HSCs but failed to restore their proper function. Consequently, approximately 60% of $Nras^{G12D/G12D}$ mice treated with MEK inhibitor alone died within 20 weeks, and the remaining animals continued to display JMML/MP-CMML–like phenotypes. In contrast, combined inhibition of MEK and JAK/STAT signaling, which is commonly hyperactivated in human and mouse CMML, potently inhibited human and mouse CMML cell growth in vitro, rescued mutant $Nras^{G12D/G12D}$-expressing HSC function in vivo, and promoted long-term survival without evident disease manifestation in $Nras^{G12D/G12D}$ animals. These results provide a strong rationale for further exploration of combined targeting of MEK/ERK and JAK/STAT in treating patients with JMML and MP-CMML.

Combined MEK and JAK inhibition abrogates murine myeloproliferative neoplasm

Guangyao Kong,[1] Mark Wunderlich,[2] David Yang,[3] Erik A. Ranheim,[3] Ken H. Young,[4] Jinyong Wang,[1] Yuan-I Chang,[1] Juan Du,[1] Yangang Liu,[1] Sin Ruow Tey,[5] Xinmin Zhang,[6] Mark Juckett,[7] Ryan Mattison,[7] Alisa Damnernsawad,[1] Jingfang Zhang,[1] James C. Mulloy,[2] and Jing Zhang[1]

[1]McArdle Laboratory for Cancer Research, University of Wisconsin-Madison, Madison, Wisconsin, USA.
[2]Department of Pediatrics, Cincinnati Children's Hospital Medical Center, Cincinnati, Ohio, USA.
[3]Department of Pathology and Laboratory Medicine, University of Wisconsin School of Medicine and Public Health, University of Wisconsin Carbone Cancer Center (UWCCC), Madison, Wisconsin, USA.
[4]Department of Hematopathology, University of Texas MD Anderson Cancer Center, Houston, Texas, USA.
[5]Department of Genetics, University of Wisconsin-Madison, Madison, Wisconsin, USA. [6]BioInfoRx Inc., Madison, Wisconsin, USA.
[7]Department of Medicine, University of Wisconsin School of Medicine and Public Health, UWCCC, Madison, Wisconsin, USA.

Overactive RAS signaling is prevalent in juvenile myelomonocytic leukemia (JMML) and the myeloproliferative variant of chronic myelomonocytic leukemia (MP-CMML) in humans, and both are refractory to conventional chemotherapy. Conditional activation of a constitutively active oncogenic *Nras* (*Nras*$^{G12D/G12D}$) in murine hematopoietic cells promotes an acute myeloproliferative neoplasm (MPN) that recapitulates many features of JMML and MP-CMML. We found that *Nras*$^{G12D/G12D}$-expressing HSCs, which serve as JMML/MP-CMML–initiating cells, show strong hyperactivation of ERK1/2, promoting hyperproliferation and depletion of HSCs and expansion of downstream progenitors. Inhibition of the MEK pathway alone prolonged the presence of *Nras*$^{G12D/G12D}$-expressing HSCs but failed to restore their proper function. Consequently, approximately 60% of *Nras*$^{G12D/G12D}$ mice treated with MEK inhibitor alone died within 20 weeks, and the remaining animals continued to display JMML/MP-CMML–like phenotypes. In contrast, combined inhibition of MEK and JAK/STAT signaling, which is commonly hyperactivated in human and mouse CMML, potently inhibited human and mouse CMML cell growth in vitro, rescued mutant *Nras*$^{G12D/G12D}$-expressing HSC function in vivo, and promoted long-term survival without evident disease manifestation in *Nras*$^{G12D/G12D}$ animals. These results provide a strong rationale for further exploration of combined targeting of MEK/ERK and JAK/STAT in treating patients with JMML and MP-CMML.

Introduction

Hyperactive RAS signaling has been implicated in both juvenile myelomonocytic leukemia (JMML) and the myeloproliferative variant of chronic myelomonocytic leukemia (MP-CMML), with mutations in the *NRAS* or *KRAS* oncogenes and their downstream or regulatory molecules collectively identified in approximately 90% of JMML and approximately 50% of MP-CMML patients (1). Significantly, acquisition of 2 copies of oncogenic *RAS* alleles, including *NRAS*$^{G12D/G12D}$ and *KRAS*$^{G13D/G13D}$, is associated with JMML/CMML progression in humans and mice (COSMIC database and refs. 2–5), which indicates that incremental activation of RAS signaling is a pathological mechanism contributing to JMML/CMML development. JMML and CMML patients respond poorly to conventional chemotherapy, and only BM transplantation significantly prolongs their survival. These observations prompt intensive efforts to develop various therapeutic approaches to target overactive RAS signaling for treating JMML and CMML (6). It has proven difficult to develop compounds that directly inhibit oncogenic *RAS*. Therefore, widespread investigation has been focusing on targeting the downstream RAS signaling network that promotes leukemogenesis.

We and other laboratories previously developed 3 genetically engineered mouse models that express 1 or 2 copies of constitutively active *Nras*^{G12D} or 1 copy of *Kras*^{G12D} in the hematopoietic compartment (*Nras*$^{G12D/+}$, *Nras*$^{G12D/G12D}$, or *Kras*$^{G12D/+}$, respectively) (4, 7–13). All 3 models recapitulate many features of human JMML/MP-CMML, either acutely or chronically. The initiation and progression of JMML/MP-CMML phenotypes are tightly associated with ERK1/2 hyperactivation in hematopoietic stem/progenitor cells (HSPCs). These studies suggest that the MEK/ERK pathway is a driving force in oncogenic *RAS*–induced JMML/MP-CMML. Consistent with this idea, a MEK inhibitor controls JMML/MP-CMML–like phenotypes in *Kras*$^{G12D/+}$ and *Nf1*$^{-/-}$ mice (14, 15).

Despite the short-term effectiveness of MEK inhibitors in treating various cancers in preclinical and clinical settings, acquired resistance to these inhibitors has been well documented in long-term studies (15–18). The acquired resistance to MEK inhibitors is partially attributed to genetic and epigenetic changes that further promote hyperactivation of the RAS/MEK/ERK pathway, for example, upregulation of positive regulators of RAS signaling (17) and acquired genetic mutations in the *MEK* and *RAS* genes (19, 20). However, in other cases, acquired resistance to MEK inhibitors is associated with cancer-initiating cells. For instance, in the *Kras*$^{G12D/+}$-induced JMML/MP-CMML model, mutant HSCs serve as leukemia-initiating cells (9, 21). Although a MEK inhibitor effectively controls JMML/MP-CMML phenotypes, it is not very effective in restoring the function of mutant HSCs, which promote a lethal T cell leukemia (14). Therefore, we sought a combined therapy to more effectively restore mutant HSC function and overcome resistance to MEK inhibitors.

Conflict of interest: The authors have declared that no conflict of interest exists.
Citation for this article: *J Clin Invest.* 2014;124(6):2762–2773. doi:10.1172/JCI74182.

Detailed signaling studies in oncogenic *Ras* models have shown that in addition to the MEK/ERK pathway, overactivity of the JAK/STAT pathway is also involved in the pathogenesis of JMML/MP-CMML, while hyperactivation of AKT is not detected (4, 10, 13, 22). Although *JAK2* mutations are extremely rare in JMML and CMML, robust hyperactivation of the JAK/STAT pathway was previously reported in JMML and CMML patient samples (23). Thus, we hypothesized that the JAK/STAT pathway plays an important role in JMML/CMML development, constituting a leukemic cell–addicted pathway. We tested this hypothesis in our $Nras^{G12D/G12D}$ model because unlike in $Kras^{G12D/+}$ mice (8), 100% of $Nras^{G12D/G12D}$ mice die of severe JMML/MP-CMML without the complications of hyperplasia phenotypes in other tissues (12).

Here, we found that endogenous $Nras^{G12D/G12D}$ signaling hyperactivated ERK1/2, but not AKT, in HSCs and promoted their hyperproliferation and subsequent depletion. Concomitantly, downstream progenitor cells underwent great expansion. Depletion of $Nras^{G12D/G12D}$ HSCs was not associated with overexpression of cell senescence genes and was rescued by short-term treatment with the MEK inhibitor AZD6244, but not with rapamycin. Side-by-side comparison of combined MEK and JAK inhibition with single-pathway inhibition indicated that the combination treatment not only more effectively inhibited the growth of human and mouse CMML cells in vitro, but also provided long-term rescue of mutant HSC function in vivo where single-pathway inhibition failed. All $Nras^{G12D/G12D}$ mice that underwent combination treatment survived without significant disease phenotypes. Therefore, our results provide a rationale for performing clinical trials of MEK inhibitors and JAK inhibitors used in combination to treat JMML and CMML patients.

Results

$Nras^{G12D/G12D}$ HSCs undergo hyperproliferation and become depleted. Because oncogenic *RAS*–expressing HSCs appear to serve as JMML/MP-CMML–initiating cells (12, 24), we investigated how endogenous $Nras^{G12D/G12D}$ affects HSC functions to promote leukemogenesis. HSCs were defined herein as $Lin^-CD41^-CD48^-cKit^+Sca1^+CD150^+$. We first examined the HSC compartment in $Nras^{G12D/G12D}$ *Mx1-Cre* mice (11) at different time points after injections with polyinosinic-polycytidylic acid (pI-pC). On days 5 and 12 relative to the day of the first pI-pC injection (day 1), the frequency and absolute number of $Nras^{G12D/G12D}$ HSCs continuously decreased compared with control HSCs (Figure 1A). The total number of multipotent progenitors (MPPs) in $Nras^{G12D/G12D}$ mice was concomitantly decreased compared with that in control mice, whereas the $Lin^-Sca1^+cKit^+$ (LSK) compartment, especially $CD48^+$ LSK cells, was significantly expanded compared with controls (Figure 1, B and C, and Supplemental Figure 1; supplemental material available online with this article; doi:10.1172/JCI74182DS1).

Expression of endogenous $Nras^{G12D/G12D}$ increased the division of HSCs, but not whole BM (WBM) cells (Figure 1, D–F). On day 12, consistent with a previous report (25), more than 90% of control HSCs were in G0 stage and only approximately 0.5%–1% were in S/G2/M stage. In contrast, a significant decrease of $Nras^{G12D/G12D}$ HSCs was detected in G0 stage as well as a concomitant increase in G1 and S/G2/M stages (Figure 1D), suggestive of increased proliferation in mutant HSCs. This result was further confirmed using EdU in vivo incorporation (Figure 1F). The increased proliferation in $Nras^{G12D/G12D}$ HSCs was similar to that previously observed in $Kras^{G12D/+}$ HSCs (13), but much greater than reported in $Nras^{G12D/+}$ HSCs (24).

To determine whether the proliferation of $Nras^{G12D/G12D}$ HSCs is correlated with decreased HSC self-renewal, we transplanted highly purified control or $Nras^{G12D/G12D}$ HSCs along with WT WBM cells into lethally irradiated mice. Compared with control cells, $Nras^{G12D/G12D}$-derived blood cells were significantly reduced in peripheral blood (PB) of recipients (Figure 1G). We sacrificed the recipients 12 weeks after transplant. Control donor HSCs represented approximately 26% of the recipients' BM HSC compartment, while $Nras^{G12D/G12D}$ HSCs represented approximately 8% (Figure 1H). These results indicate that $Nras^{G12D/G12D}$ signaling decreases HSC self-renewal capability and depletes the HSC compartment.

To better understand the molecular mechanisms underlying endogenous $Nras^{G12D/G12D}$ signaling–induced aberrant HSC function, we performed microarray analysis using highly purified HSCs. Compared with control HSCs, $Nras^{G12D/G12D}$ HSCs did not show significant differential expression of genes associated with HSC self-renewal (Supplemental Figure 2A and ref. 26) or a negative enrichment of HSC self-renewal signature (Supplemental Figure 2B and ref. 27). Further gene set enrichment analysis (GSEA) of our HSC microarray results identified a gene signature associated with lymphoid differentiation in $Nras^{G12D/G12D}$ HSCs (Supplemental Figure 2C). Consistent with the GSEA results, the common lymphoid progenitor cell (CLP) compartment was greatly expanded in $Nras^{G12D/G12D}$ mice, in addition to the expansion of the common myeloid progenitor cell (CMP) compartment (Supplemental Figure 2, D and E).

ERK1/2 is hyperactivated in $Nras^{G12D/G12D}$ HSCs, and downregulation of MEK/ERK signaling rescues the depletion of $Nras^{G12D/G12D}$ HSCs. We investigated whether the depletion of $Nras^{G12D/G12D}$ HSCs is associated with hyperactivation of ERK1/2. In the absence of cytokines, ERK1/2 was substantially hyperactivated in $Nras^{G12D/G12D}$ HSCs (~3-fold over control HSCs), but only marginally hyperactivated in $Nras^{G12D/G12D}$ MPPs (~1.2 fold over control MPPs) (Figure 2A). This is likely due to the distinct, yet unknown, signaling regulatory mechanisms in HSCs and MPPs. As expected (24), hyperactivation of ERK1/2 in $Nras^{G12D/G12D}$ HSCs was markedly stronger than that in $Nras^{G12D/+}$ HSCs (3- and 2-fold, respectively, over control HSCs). In contrast, AKT and STAT5 activation in $Nras^{G12D/G12D}$ HSCs and MPPs was comparable to that in controls (Figure 2A and Supplemental Figure 4B). Upon stimulation with IL-3, ERK1/2 was not further hyperactivated in $Nras^{G12D/G12D}$ HSCs or MPPs compared with their respective controls; the response curves were shifted up merely due to the constitutive activation of ERK1/2 (Figure 2B). Despite the strong hyperactivation of ERK1/2, we did not find significant upregulation of c-Myc and cell senescence genes (e.g., *p53*, $p16^{INK4a}$, and $p15^{INK4b}$) in $Nras^{G12D/G12D}$ HSCs (Figure 2C). Our data suggest that, unlike the prevailing theory based on RAS overexpression studies (28), depletion of $Nras^{G12D/G12D}$ HSCs is not caused by cell senescence.

To test whether hyperactivation of MEK/ERK signaling contributes to $Nras^{G12D/G12D}$ HSC depletion, we treated control and $Nras^{G12D/G12D}$ mice with vehicle or AZD6244 (29, 30), an efficacious and specific MEK inhibitor (24). AZD6244 treatment rescued depletion of $Nras^{G12D/G12D}$ HSCs to a level comparable to control HSCs (Figure 2D). The identity of these rescued HSCs was further confirmed by genotyping single HSCs (Figure 2E). As a control, we treated $Nras^{G12D/G12D}$ mice with rapamycin, an inhibitor of the mTOR/AKT pathway, which rescues HSC defects in *Pten*-deficient mice (25). Consis-

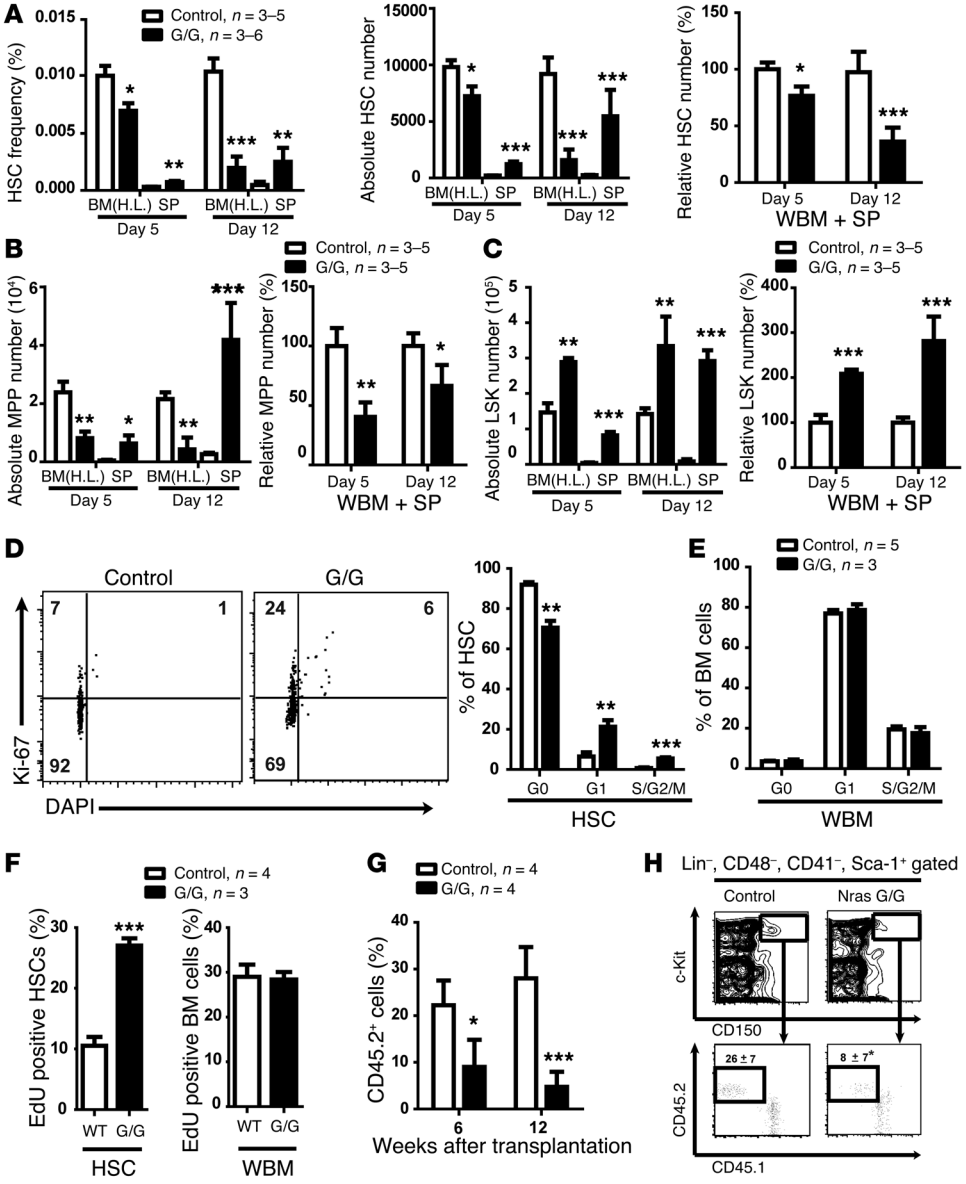

Figure 1

Endogenous *Nras*$^{G12D/G12D}$ induces hyperproliferation, decreased self-renewal, and depletion of HSCs. (**A**–**F**) Control and *Nras*$^{G12D/G12D}$ (G/G) mice were treated with pI-pC and sacrificed at various time points (relative to the day of the first pI-pC injection, assigned as day 1) for analysis. Lin$^-$CD41$^-$CD48$^-$cKit$^+$Sca1$^+$CD150$^+$ HSCs (**A**), Lin$^-$CD41$^-$CD48$^-$cKit$^+$Sca1$^+$CD150$^-$ MPPs (**B**), and LSK cells (**C**) were quantified using flow cytometry. SP, spleen; BM(H.L.), hind limb BM content (including tibias and femurs). WBM was estimated as 4-fold the hind limb BM value (42). (**D** and **E**) Cell cycle analysis of HSCs (**D**) and WBM (**E**) from control and *Nras*$^{G12D/G12D}$ mice using Ki67/DAPI staining on day 12. (**F**) A 16-hour pulse of EdU to quantify proliferating HSCs and WBM. (**G**) 20 HSCs purified from control or *Nras*$^{G12D/G12D}$ mice were transplanted with 2 × 10^5 congeneic BM cells into lethally irradiated mice. Donor-derived blood cells were regularly analyzed in the PB of recipients. (**H**) Donor-derived HSCs were quantified in recipients 12 weeks after transplantation. Data are mean ± SD. *P < 0.05; **P < 0.01; ***P < 0.001.

tent with our HSC signaling study, rapamycin failed to rescue HSC depletion in *Nras*$^{G12D/G12D}$ mice (Supplemental Figure 3). Moreover, rapamycin failed to rescue the expansion of CMP and CLP compartments in *Nras*$^{G12D/G12D}$ mice. These results suggested that MEK/ERK signaling is the major driving force of *Nras*$^{G12D/G12D}$ HSC phenotypes.

Combined inhibition of JAK and MEK effectively controls mouse and human CMML cell growth in vitro. Since acquired resistance to MEK inhibitors has been well documented in long-term studies, we were motivated to search for a combination therapy to overcome this resistance. We noted that hyperactivation of STAT5 in HSPCs or MPPs was associated with oncogenic *Ras*–induced JMML/MP-CMML (Supplemental Figure 4 and refs. 4, 13, 22), and IL-6–evoked STAT3 activation in *Nras*$^{G12D/G12D}$ HSPCs was also mediated by JAK (Supplemental Figure 5). Therefore, we investigated whether combined inhibition of JAK/STAT and MEK/ERK would effectively treat oncogenic *Ras*–induced leukemias.

We chose to use AZD1480, a potent JAK2 inhibitor that also inhibits JAK1 and JAK3 (31). At a high concentration (5 μM), AZD1480 alone or combined with AZD6244 specifically and potently blocked GM-CSF–evoked ERK1/2 and STAT5 activation without affecting SCF-evoked AKT activation, whereas AZD6244 alone only inhibited GM-CSF–evoked ERK1/2 activation (Figure 3A). However, when used at a 10-fold lower concentration, only the combination of AZD6244 and AZD1480 completely blocked GM-CSF–evoked ERK1/2 activation; each drug alone achieved only partial inhibition (Supplemental Figure 6). Our results demonstrated that combination AZD6244 and AZD1480 efficaciously and specifically blocks both JAK/STAT and MEK/ERK pathways.

To determine whether combined inhibition of JAK/STAT and MEK/ERK effectively inhibits CMML cell growth in vitro, we isolated leukemia cells from moribund *Nras*$^{G12D/G12D}$ mice and cultured them in vitro in the presence or absence of the inhibitors. CellTiter-Glo assay was performed to evaluate cell viability. Our

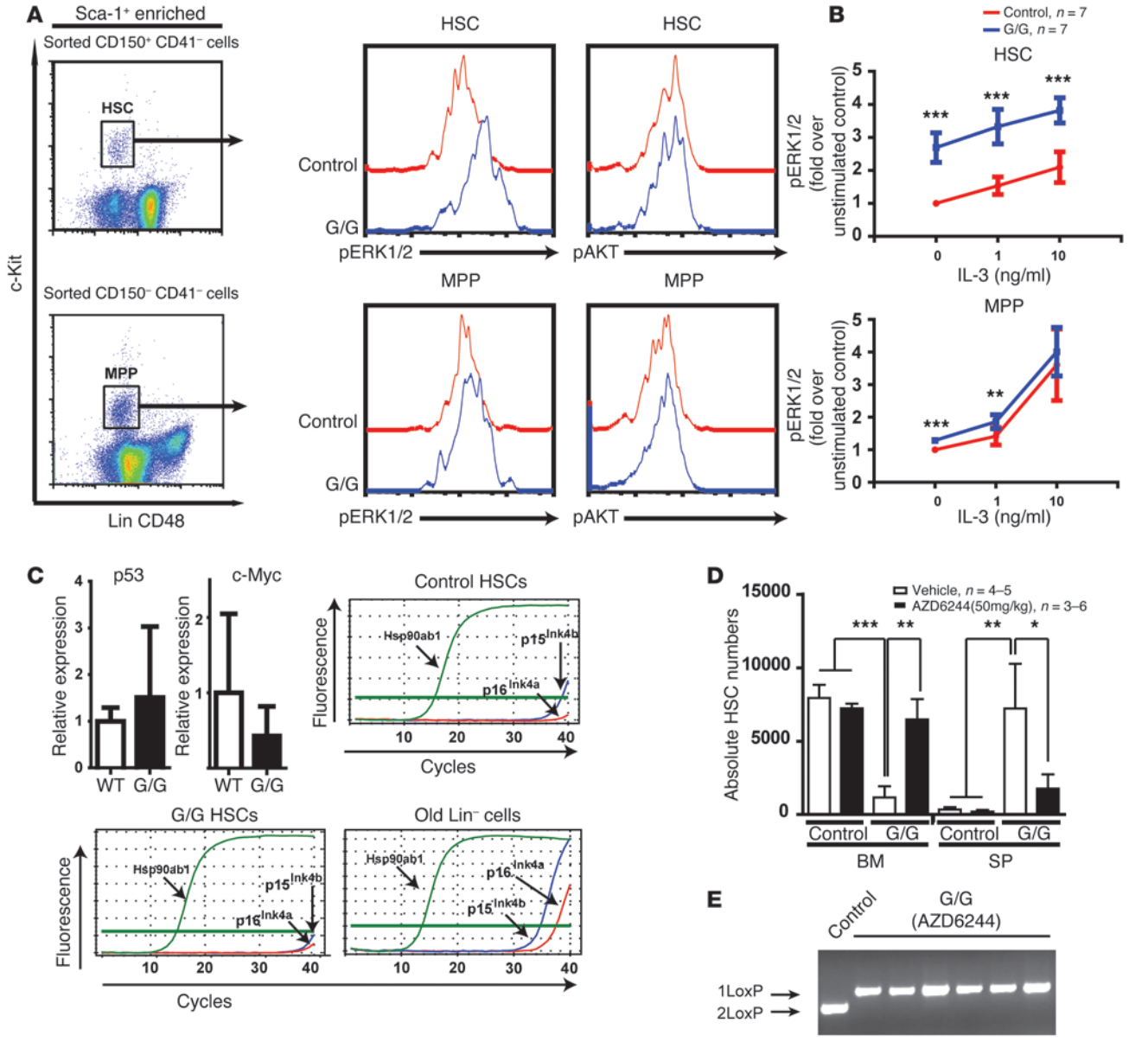

Figure 2

Nras$^{G12D/G12D}$ hyperactivates ERK1/2 in HSCs, and downregulation of MEK/ERK signaling rescues *Nras*$^{G12D/G12D}$ HSC exhaustion. Control and *Nras*$^{G12D/G12D}$ mice were treated with pI-pC and sacrificed on day 12. (**A** and **B**) CD150^{+}CD41^{-} cells (enriched for HSCs) and CD150^{-}CD41^{-} cells (enriched for MPPs) were sorted from Sca1^{+}-enriched total BM cells. Sorted cells were serum and cytokine starved for 30 minutes at 37°C (**A**). IL-3 stimulation was performed for 10 minutes at 37°C after starvation (**B**). Levels of pERK1/2 and pAKT were measured using phosphospecific flow cytometry. HSCs (defined as [Lin CD48]$^{-/lo}$cKit^{+} cells from sorted CD150^{+}CD41^{-} cells) and MPPs (defined as [Lin CD48]$^{-/lo}$cKit^{+} cells from sorted CD150^{-}CD41^{-} cells) were gated for data analysis. To quantify the activation of ERK1/2, median intensities of pERK1/2 at different IL-3 concentrations are shown relative to the respective control cells at 0 ng/ml (assigned as 1). (**C**) Quantification of c-Myc and cell senescence–related genes in control and *Nras*$^{G12D/G12D}$ HSCs using qRT-PCR. (**D**) Quantification of BM spleen HSCs from control and *Nras*$^{G12D/G12D}$ mice treated with vehicle or AZD6244 for 7 days. (**E**) Single *Nras*$^{G12D/G12D}$ HSC genotyping after AZD6244 treatment. Data are mean ± SD. $^{*}P < 0.05$; $^{**}P < 0.01$; $^{***}P < 0.001$.

results demonstrated that the 2 compounds successfully inhibited leukemia cell growth in vitro (Figure 3B). The efficacy of this drug combination was significantly better than AZD6244 or AZD1480 alone and was also considerably better than U0126 and AG490, the old-generation inhibitors of MEK and JAK2, respectively (used at higher doses in the parallel study). Similarly, combination AZD6244 and AZD1480 effectively inhibited growth of JMML/MP-CMML cells isolated from moribund *Kras*$^{G12D/+}$ mice and recipients transplanted with *Nras*$^{G12D/+}$ cells (Figure 3B). These results were further confirmed in human CMML cells. Combined AZD6244 and AZD1480 potently blocked human GM-CSF–evoked ERK1/2 and STAT5 activation (Supplemental

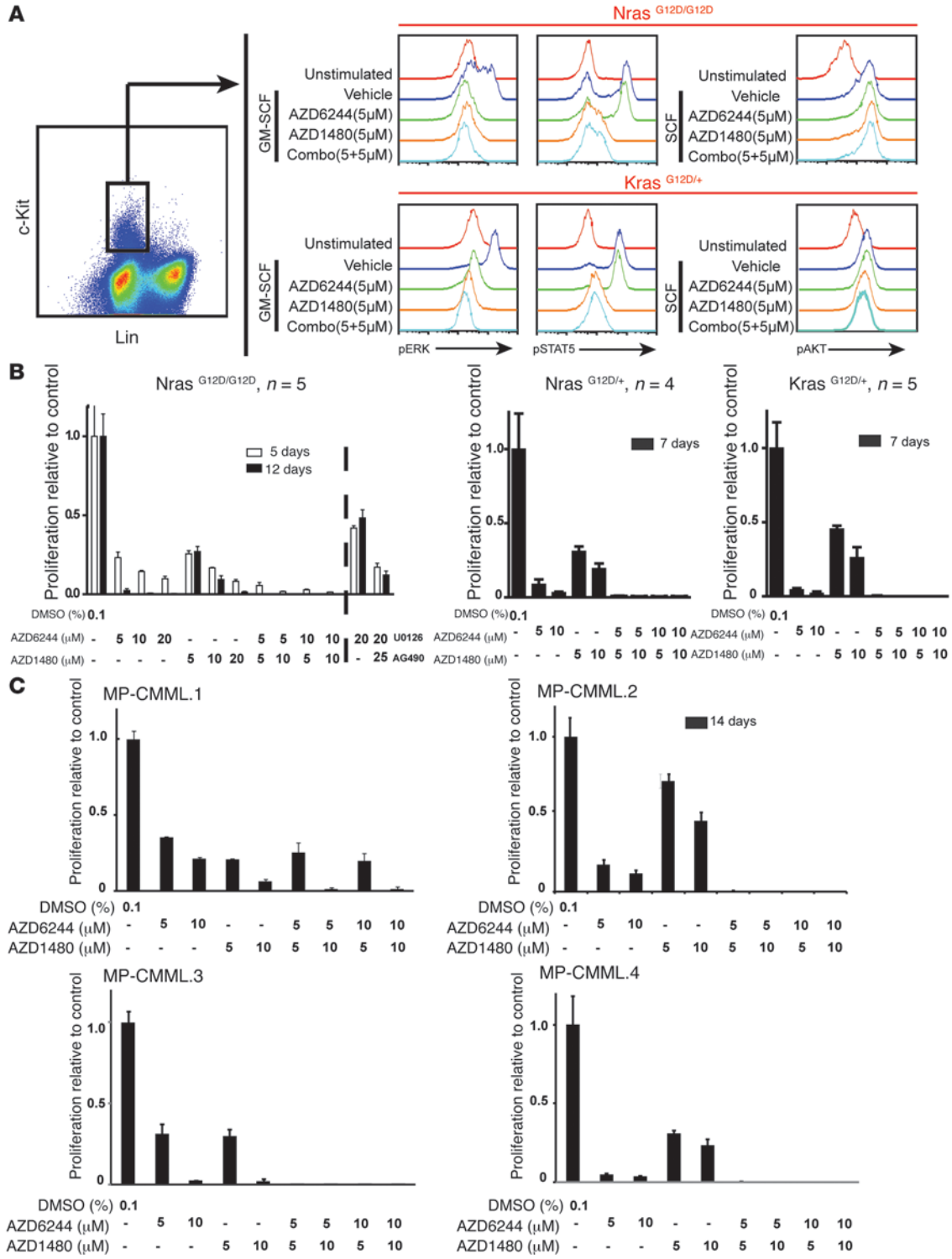

Figure 3

Combined inhibition of JAK and MEK effectively blocks the growth of human and mouse JMML/MP-CMML cells in vitro. (**A**) WBM cells from moribund *Nras*$^{G12D/G12D}$ or *Kras*$^{G12D/+}$ mice with advanced JMML/MP-CMML were serum and cytokine starved for 90 minutes at 37°C and incubated with DMSO vehicle or drugs for another 30 minutes at 37°C. Cells were then stimulated with 10 ng/ml GM-CSF or SCF for 10 minutes at 37°C. Levels of pERK1/2, pSTAT5, and pAKT were measured using phosphospecific flow cytometry. Non-neutrophil Lin$^-$cKit$^+$ cells were gated for data analysis. Shown are results of 1 representative experiment. (**B** and **C**) BM cells from moribund *Nras*$^{G12D/G12D}$, *Nras*$^{G12D/+}$, and *Kras*$^{G12D/+}$ mice with advanced JMML/MP-CMML (**B**) and from human MP-CMML patients (**C**; $n = 5$) were cultured in triplicate in 96-well plates in the presence of vehicle or various concentrations of AZD6244 and/or AZD1480 for 5–14 days. Cell number was quantified by CellTiter-Glo assay. Data are mean ± SD.

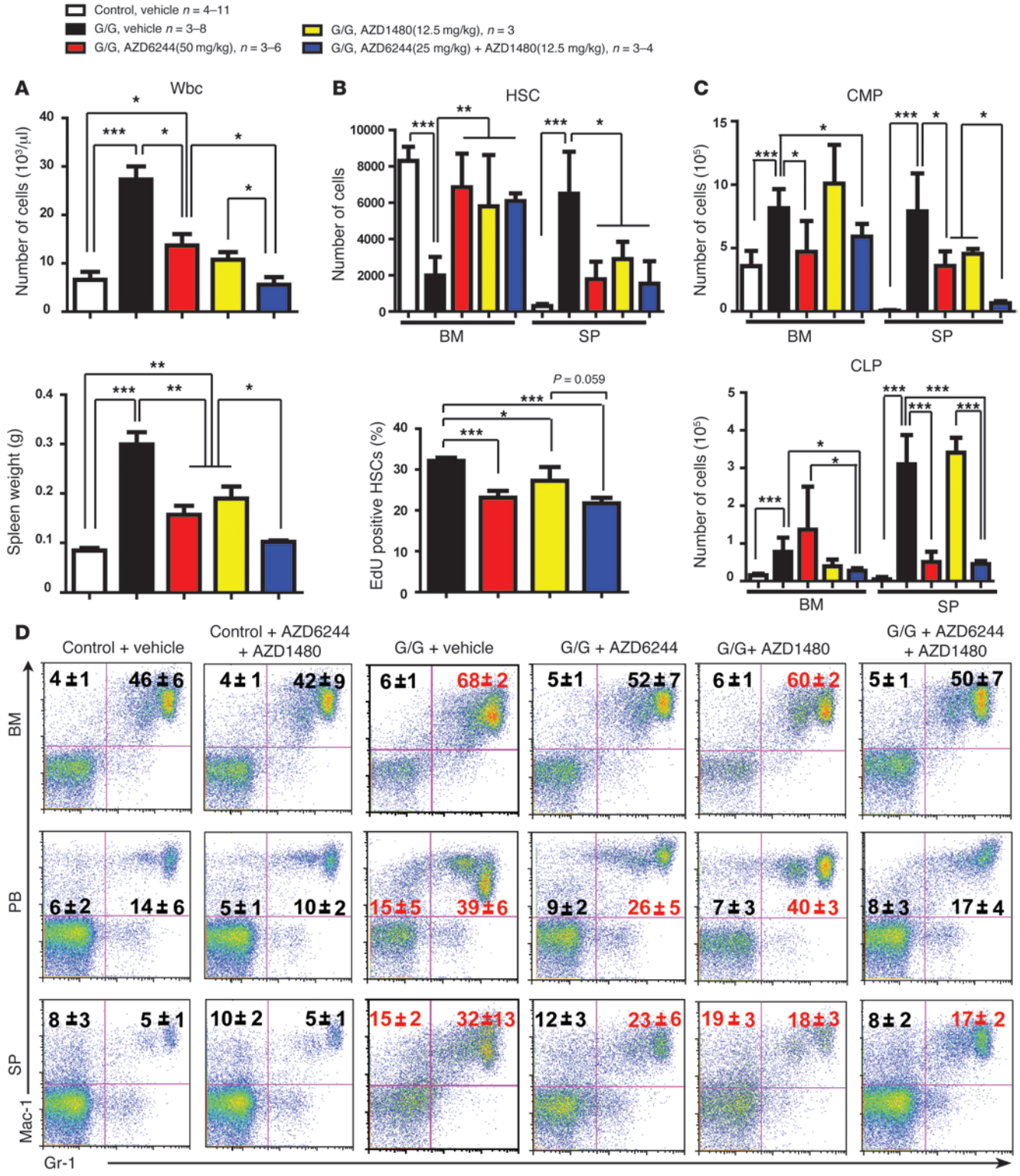

Figure 4

Combined inhibition of JAK and MEK effectively controls the JMML/MP-CMML phenotypes in *Nras*$^{G12D/G12D}$ mice. Control and *Nras*$^{G12D/G12D}$ mice were injected with pI-pC and then treated with vehicle, AZD6244, and/or AZD1480 from day 5 to day 12. (**A**) wbc number in PB and spleen weight. (**B**) Number of total HSCs and cycling HSCs (labeled with EdU-containing water [0.5 mg/ml] for the last 16 hours of drug treatment). (**C**) Number of CMPs and CLPs in BM and spleen. (**D**) Flow cytometric analysis of PB, spleen, and BM cells using myeloid lineage–specific markers. Debris and unlysed rbcs (low forward scatter) and dead cells (propidium iodide positive) were excluded from analysis. Significant differences from vehicle-treated controls ($P < 0.05$) are denoted by red font. Data are mean ± SD. *$P < 0.05$; **$P < 0.01$; ***$P < 0.001$.

Figure 7) and inhibited the in vitro growth of human CMML cells (n = 5) (Figure 3C). Together, these results indicated that combined inhibition of JAK/STAT and MEK/ERK effectively controls both human and mouse CMML cell growth in vitro.

Combined inhibition of JAK and MEK prevents JMML/MP-CMML–like phenotypes in $Nras^{G12D/G12D}$ mice. We treated $Nras^{G12D/G12D}$ mice immediately after oncogenic *Nras* induction with vehicle, AZD6244, and/or AZD1480 for 7 days to determine whether combined inhibition of JAK and MEK in vivo more effectively controls JMML/MP-CMML–like phenotypes than single-pathway inhibition. We used the published safe doses for AZD6244 alone (50 mg/kg; refs. 29, 30) and AZD1480 alone (12.5 mg/kg; ref. 31). A safe dose of combination AZD6244 (25 mg/kg) and AZD1480 (12.5 mg/kg) was determined in vivo (Supplemental Figure 8), which indicates that the effects of the drug combination are not generally myelosuppressive. Our results showed that single-pathway inhibition indeed significantly attenuated leukemia phenotypes in vivo, as shown by lower wbc counts in PB, reduced splenomegaly, rescued HSC exhaustion, and various degrees of reduction in CMP and CLP compartments in BM and/or spleen (Figure 4, A–C). However, significant myelopoiesis remained in various hematopoietic tissues (Figure 4D). In contrast, combined inhibition of JAK and MEK more effectively controlled JMML/MP-CMML phenotypes in vivo and corrected almost all the parameters to levels seen in control mice. These data suggested that combination AZD6244 and AZD1480 treats early-stage JMML/MP-CMML more effectively than single drugs.

Combined inhibition of JAK and MEK provides long-term survival in diseased $Nras^{G12D/G12D}$ mice. We further investigated whether combined inhibition of JAK and MEK would effectively and sustainably treat advanced JMML/MP-CMML phenotypes in $Nras^{G12D/G12D}$ mice. $Nras^{G12D/G12D}$ mice with wbc counts above 40×10^3 cells/μl were treated with vehicle, AZD6244 alone (2 different doses), AZD1480 alone, or AZD6244 and AZD1480 combined. Treated mice were closely monitored for signs of hematopoietic malignancies (Figure 5). The treatment was terminated either when treated mice became moribund or at the end of 20 weeks. All animals treated with vehicle (n = 10) died within 8 weeks with severe JMML/MP-CMML (Figure 5A). Analysis of moribund animals showed greatly elevated wbc counts, huge spleens filled with myelomonocytic cells, and moderately enlarged thymi (indicative of an early stage of T cell disease) (Figure 6). The absolute numbers of HSCs were low, but CMP and CLP compartments were expanded.

We did not observe significant differences in $Nras^{G12D/G12D}$ mice treated with either low-dose (n = 10) or high-dose (n = 6) AZD6244. Both doses effectively rescued phenotypes of anemia and thrombocytopenia (Figure 5, C–F). However, neither dose restored wbc counts to levels comparable to those of control mice (Figure 5B). Consequently, approximately 60% of the treated mice died of JMML/MP-CMML with or without acute T cell lymphoblastic leukemia/lymphoma (T-ALL) within 20 weeks, and the mice that survived until the end of the 20-week treatment displayed significant phenotypes of JMML/MP-CMML and an early stage of T-ALL (Figure 6). $Nras^{G12D/G12D}$ mice treated with AZD1480 alone (n = 9) showed survival and leukemia phenotypes similar to those of $Nras^{G12D/G12D}$ mice treated with AZD6244 alone, except that platelet counts in AZD1480-treated mice remained low, and thymus weights were comparable to those in WT control mice (Figure 6). Together, our data indicated that neither AZD6244 nor AZD1480 alone effectively provides disease-free long-term survival in $Nras^{G12D/G12D}$ mice.

In contrast to mice treated with AZD6244 or AZD1480 alone, all $Nras^{G12D/G12D}$ mice treated with combination AZD6244 and AZD1480 (n = 9) survived and were overtly healthy (Figures 5 and 6). Their wbc, rbc, and platelet counts were stably maintained at levels comparable to those in control mice (Figure 5, B–F). Detailed analysis of their hematopoietic tissues demonstrated that their spleen weights and gross structures were indistinguishable from those in controls, and their thymus weights were normal (Figure 6, B, C, and G). Therefore, we concluded that combination AZD6244 and AZD1480 effectively controls JMML/MP-CMML and T-ALL development and allows long-term survival in $Nras^{G12D/G12D}$ mice.

To validate our mouse results in a human leukemia model, we attempted to establish stable engraftment of human CMML cells in immunocompromised mice expressing human cytokines (NSGS mice) (32). We transplanted 8 CMML samples into NSGS mice; 4 samples showed unstable, fluctuating human grafts over a 6-month period (Supplemental Figure 9). The mouse engrafted with CMML-20 had to be sacrificed at 10 weeks due to illness. The BM from this mouse was transplanted into secondary mice, none of which showed significant human cell engraftment. Therefore, this approach did not efficiently generate a preclinical model that could be used to test the combination treatment. The results of the human engraftment model were consistent with our previously reported mouse data, in which JMML/MP-CMML phenotypes appear to be driven by waves of clonal expansion of myeloid cells in the short term, but require initiation and maintenance by mutant HSCs over the long term (24).

Combined inhibition of JAK and MEK sustainably attenuates $Nras^{G12D/G12D}$ HSC phenotypes. To determine whether combination AZD6244 and AZD1480 effectively treats leukemia in $Nras^{G12D/G12D}$ mice by eliminating mutant HSCs, which serve as leukemia-initiating cells in oncogenic *RAS* models (9, 12, 13, 24), we analyzed HSCs and their downstream progenitors after short-term (7 days) and long-term (20 weeks) treatments. Interestingly, although AZD6244 reduced HSC cycling and rescued $Nras^{G12D/G12D}$ HSC depletion in the short term (Figure 4B), the mutant HSCs were eventually exhausted during long-term treatment (Figure 6D). The expansion of the CMP compartment in BM was transiently controlled, whereas the CLP compartment remained expanded in BM, similar to vehicle-treated $Nras^{G12D/G12D}$ mice, throughout the treatment. In these studies, AZD1480 exerted similar or less dramatic effects on mutant HSCs, CMPs, and CLPs compared with AZD6244 (Figure 4, B and C, and Figure 6, D–F). To our surprise, short-term treatment with combination AZD6244 and AZD1480 significantly reduced cycling of mutant HSCs and rescued their depletion to the same extent as the single-drug treatments (Figure 4B). However, in sharp contrast to single-drug treatments, combination treatment effectively controlled the expansion of both CMP and CLP compartments (Figure 4C). More importantly, these effects lasted over the long term (Figure 6D and Supplemental Figure 10). We further excluded the possibility that the in vivo potency of the combination treatment was through silencing or downregulating oncogenic *Nras* expression (Supplemental Figure 11). Rather, our results suggest that the combination treatment effectively controlled the leukemogenic signaling network and restored, at least in part, the normal function of $Nras^{G12D/G12D}$ HSCs.

To test this, we transplanted 5×10^6 WBM cells from $Nras^{G12D/G12D}$ mice under different treatments into sublethally irradiated mice that no longer received any compounds. We reasoned that in the absence of combination AZD6244 and AZD1480, mutant HSCs

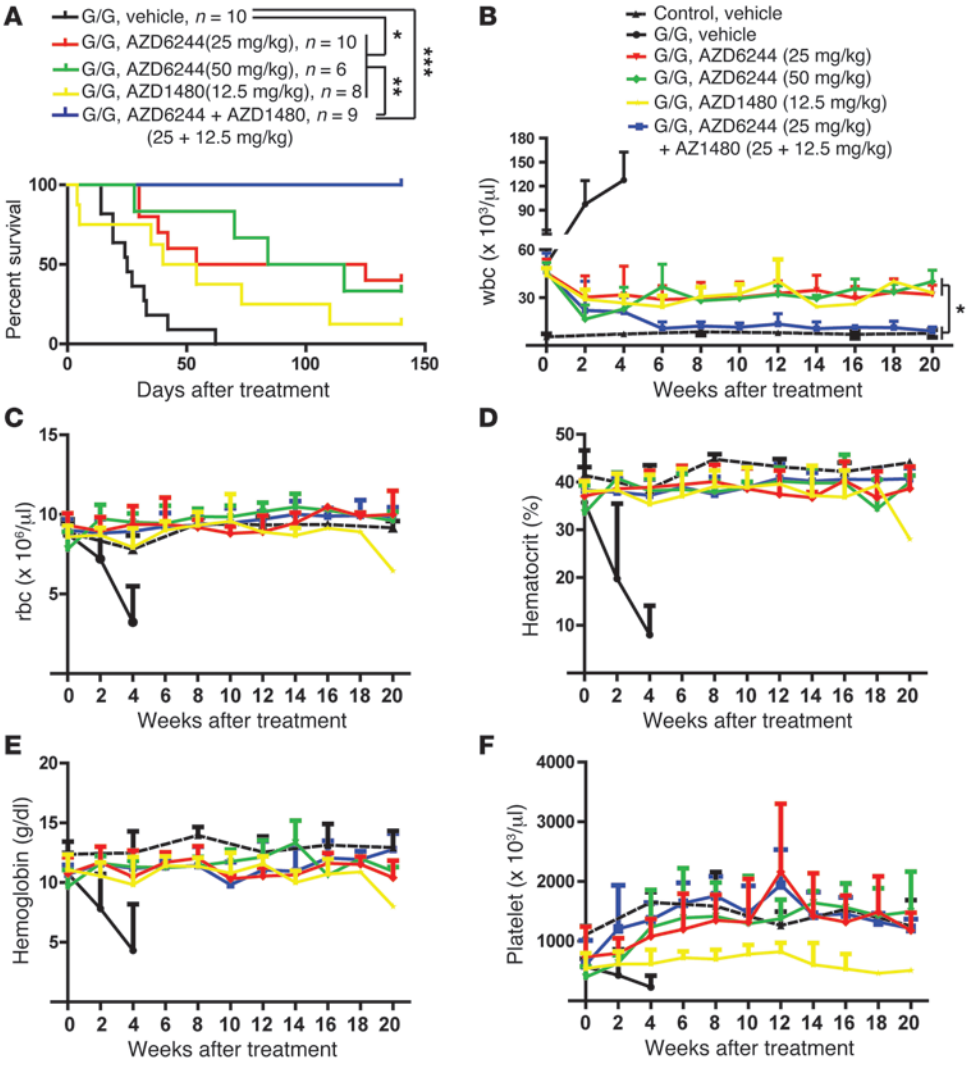

Figure 5
Combined inhibition of JAK and MEK provides long-term survival in $Nras^{G12D/G12D}$ mice. (**A**) Kaplan-Meier survival curves of $Nras^{G12D/G12D}$ mice with advanced JMML/MP-CMML treated with vehicle, AZD6244 alone, AZD1480 alone, or AZD6244 and AZD1480 combined; treatment was terminated either after 20 weeks or when mice reached a moribund stage. *P* values were determined by log-rank test. (**B**–**F**) Total wbc count (**B**), rbc count (**C**), hematocrit (**D**), hemoglobin level (**E**), and platelet count (**F**) in PB were measured every other week after treatment. Data are mean ± SD. $^{*}P < 0.05$; $^{**}P < 0.01$; $^{***}P < 0.001$.

would gradually gain their leukemia-inducing activity and thus promote hematopoietic malignancies after a prolonged latency compared with mutant HSCs treated with vehicle or single drugs. As expected, despite comparable engraftment of mutant BM cells, a highly penetrant T-ALL quickly developed in recipients transplanted with $Nras^{G12D/G12D}$ cells of mice treated with vehicle, AZD6244 alone, or AZD1480 alone, whereas the majority of recipients transplanted with $Nras^{G12D/G12D}$ cells under combination treatment developed a lethal JMML/MP-CMML and B-ALL after a significantly prolonged latency (Supplemental Figure 12). The different disease phenotypes developed in different groups of recipient mice correlated to those developed in recipients transplanted with different numbers of $Nras^{G12D/G12D}$ HSCs; low HSC numbers corresponded with predominant T-ALL, and high HSC numbers with predominant JMML/MP-CMML and B-ALL (12).

Discussion

Together, our previous and current studies demonstrated an oncogene dosage-dependent, distinct regulation of HSC functions. Endogenous $Nras^{G12D/+}$ signaling led to moderate HSC hyperproliferation, increased self-renewal, myeloid differentiation bias, and moderate hyperactivation of ERK1/2 in HSCs (24). Downregulation of MEK/ERK signaling using genetic or pharmacological approaches attenuated the mutant HSC phenotypes. In contrast, stronger hyperactivation of ERK1/2 in $Nras^{G12D/G12D}$ HSCs was associated with excessive hyperproliferation, decreased self-renewal, and depletion of HSCs. These phenotypes were alleviated upon pharmacological inhibition of MEK/ERK signaling. Interestingly, excessive hyperproliferation and depletion of HSCs were also seen in $Kras^{G12D/+}$ mice (13, 21), which express a more potent isoform of oncogenic *Ras* than do $Nras^{G12D/G12D}$ mice. Our data suggested that a quantitative change in pERK1/2 levels may lead to qualitative changes in HSC function.

Despite the differential effect of $Nras^{G12D/+}$ signaling on HSCs, results from our lab and the Morrison group suggest that targeting both MEK and JAK is also pertinent to $Nras^{G12D/+}$ HSCs (24, 33). Downregulation of *Stat5* reduces mutant HSC proliferation and aberrant self-renewal. Not surprisingly, combination AZD6244 and AZD1480 effectively inhibited growth of JMML/MP-CMML cells isolated from recipients transplanted with $Nras^{G12D/+}$ cells.

Unlike overexpression of oncogenic *Ras* in MEFs (28), expression of endogenous $Nras^{G12D/G12D}$ did not lead to overexpression of c-Myc

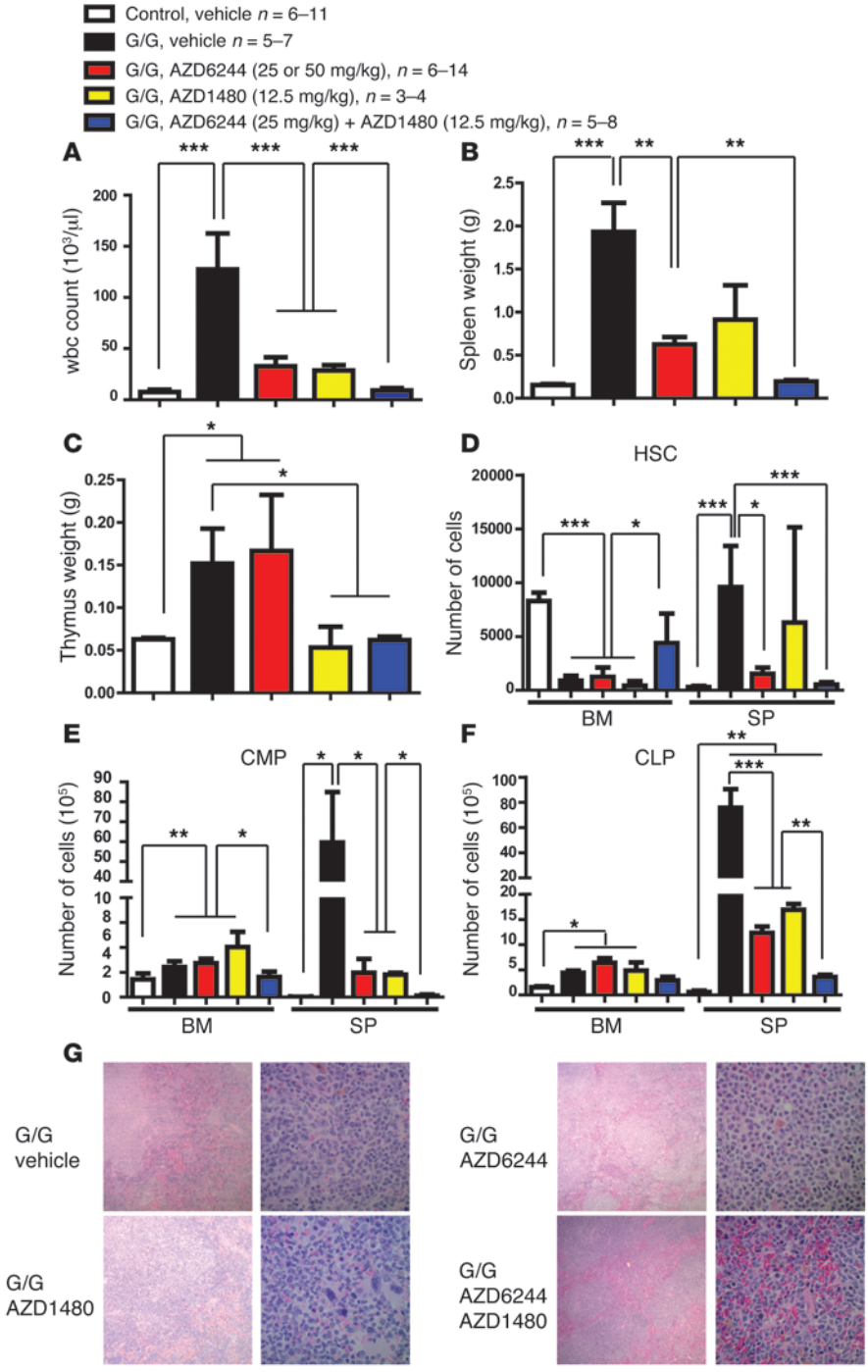

Figure 6

Combined inhibition of JAK and MEK effectively controls JMML/MP-CMML phenotypes and prevents T-ALL development in *Nras*$^{G12D/G12D}$ mice. *Nras*$^{G12D/G12D}$ mice with advanced JMML/MP-CMML were treated with vehicle, AZD6244 alone, AZD1480 alone, or AZD6244 and AZD1480 combined; treatment was terminated either after 20 weeks or when mice reached a moribund stage. (**A**–**F**) Total wbc count (**A**), spleen weight (**B**), thymus weight (**C**), HSC number (**D**), CMP number (**E**), and CLP number (**F**) in BM and spleen were quantified in different groups of animals. Because mice treated with low- or high-dose AZD6244 were essentially indistinguishable, we combined these 2 groups for data analysis. (**G**) Representative histologic H&E sections from spleen showed extensive infiltration of myelomonocytic cells and extramedullary hematopoiesis in *Nras*$^{G12D/G12D}$ mice treated with vehicle, AZD6244 alone, or AZD1480 alone, but not with AZD6244 and AZD1480 combined. Original magnification, ×4 (left); ×40 (right). Data are mean ± SD. **P* < 0.05; ***P* < 0.01; ****P* < 0.001.

or of its downstream cell senescence genes (*p53*, *p16*, and *p15*) in HSCs, which suggested that the depletion of *Nras*$^{G12D/G12D}$ HSCs is not caused by premature cell senescence. Our results were consistent with a previous report that MEFs expressing endogenous *Kras*^{G12D} do not show signs of cell senescence in long-term culture (34). Given the established role of ERK1/2 activation in regulating the balance of cell proliferation and differentiation (35–37), we propose that *Nras*$^{G12D/G12D}$ signaling results in HSC depletion mainly through hyperactivation of ERK1/2, which shifts HSC self-renewal to differentiation. Consistent with this possibility, inhibition of the MEK/ERK signaling in vivo by AZD6244 rescued the HSC depletion, while the mTOR/AKT inhibitor rapamycin did not.

Multiple mechanisms could contribute to the expansion of CMP and CLP compartments in *Nras*$^{G12D/G12D}$ mice. First, it is likely that strong *Nras*$^{G12D/G12D}$ signaling promotes expansion of these cells in a cell-autonomous manner. This possibility is supported by our previous results showing that endogenous *Nras*$^{G12D/G12D}$ causes ERK1/2 hyperactivation in myeloid progenitor–enriched HSPCs and hyperproliferation of myeloid progenitors (11). Second, the expansion of *Nras*$^{G12D/G12D}$ CMPs could also result from upstream MPPs, as the myeloid-biased, GM-CSF–responsive fraction was greatly expanded (Supplemental Figure 4). It seems paradoxical that *Nras*$^{G12D/G12D}$ MPPs showed a myeloid differentiation bias while the mutant HSCs displayed a lymphoid differentiation bias. We postulate that the aberrant lymphoid potential in mutant MPPs is redirected toward the myeloid lineage by the action of mature *Nras*$^{G12D/G12D}$ myeloid cells, as previously reported in chronic myelogenous leukemia (38). Third, the lymphoid differentiation bias of *Nras*$^{G12D/G12D}$ HSCs might contribute to the expansion of the CLP compartment. This likely drives the highly penetrant T-ALL observed in recipients that were transplanted with low number of *Nras*$^{G12D/G12D}$ BM cells (11).

AZD6244 alone significantly prolonged the survival of diseased *Nras*$^{G12D/G12D}$ mice. The beneficial effect of this MEK inhibitor on survival was similar to that of PD0325901, a different MEK inhibitor previously used to treat other JMML/MP-CMML models (*Kras*$^{G12D/+}$ and *Nf1*$^{-/-}$ mice; refs. 14, 15). However, in all these studies, including ours, MEK inhibitors only partially controlled the JMML/MP-CMML–like phenotypes and,

consequently, a significant fraction of mice died during treatment. These results suggested that MEK inhibitors alone are insufficient to provide sustainable benefits in treating JMML/MP-CMML.

We used a high dose of AZD6244 (50 mg/kg) in the short-term study immediately after oncogenic *Nras* induction. Although the JMML/MP-CMML–like phenotypes were greatly reduced, significant abnormalities in BM and spleen remained. The early onset of drug treatment minimized the potential involvement of additional genetic mutations. Rather, our data suggest a de novo "phenotypic resistance" to AZD6244 in $Nras^{G12D/G12D}$ cells in vivo, which might result from additional uncharacterized epigenetic and/or posttranslational changes that lead to compensation of inhibited MEK. Alternatively, this phenotypic resistance might be due to MEK/ERK-independent effects of $Nras^{G12D/G12D}$ signaling. In a long-term study, we used both a low dose (25 mg/kg) and the high dose of AZD6244 in parallel in $Nras^{G12D/G12D}$ mice with advanced JMML/MP-CMML. Under these experimental settings, the de novo resistance to AZD6244 became more pronounced, with wbc counts remaining well above normal throughout the treatment.

In addition to the signaling mechanism, we believe that at the cellular level, the failure of AZD6244 to restore mutant HSC function also contributed to the development of drug resistance. As JMML/CMML-initiating cells, genetically altered HSCs dictate disease phenotypes and likely drive responses to drug treatment as well. AZD6244 treatment transiently reversed the depletion of $Nras^{G12D/G12D}$ HSCs, but failed to block CLP expansion. These effects might explain the development of T-ALL with MEK inhibitors alone, as seen in some of our $Nras^{G12D/G12D}$ mice as well as in $Kras^{G12D/+}$ mice that were similarly treated (14).

Our results indicate that leukemia phenotypes may not be eliminated by simply increasing the dose of AZD6244. Rather, simultaneously targeting the JAK/STAT pathway effectively reversed the CMP/CLP expansion effect, which was refractory to AZD6244 treatment alone. We believe that simultaneous inhibition of the JAK/STAT pathway, which plays an important role in regulating HSC self-renewal and survival, significantly contributes to the potency of this combination therapy. This likelihood is supported by a recent report showing that oncogenic *NRAS* leads to hyperphosphorylation of STAT3 and protects colorectal cancer cells from stress-induced apoptosis (39). Although AZD1480 combined with AZD6244 effectively treated $Nras^{G12D/G12D}$-induced JMML/MP-CMML, AZD1480 alone was not very effective. This is probably not surprising, as we would not expect AZD1480 to significantly affect cytokine-independent, oncogenic *Nras*–evoked MEK/ERK activation.

Based on our results, we propose the following model to explain the long-term effects of combined inhibition of the MEK/ERK and JAK/STAT pathways (Supplemental Figure 13). $Nras^{G12D/G12D}$ HSC functions were largely restored, as demonstrated by significant reduction of cycling HSCs, long-term rescue of HSC depletion, and long-term suppression of CMP and CLP compartment expansion. Consequently, $Nras^{G12D/G12D}$ mice under combination treatment survived for a long time without significant JMML/MP-CMML phenotypes. Together, our data provide a strong rationale for combined inhibition of MEK and JAK in JMML and MP-CMML.

Methods

Further information can be found in Supplemental Methods.

Mice. Mice bearing the conditional oncogenic *Nras* (Lox-stop-Lox [LSL] *Nras*) mutation were crossed to *Mx1-Cre* mice to generate LSL $Nras^{G12D/G12D}$ *Mx1-Cre* mice as previously described (11). These lines were maintained in a pure C57BL/6 genetic background (>N10).

For all short-term experiments, Cre expression was induced by 2 i.p. injections of pI-pC (7.5 μg/g body weight; GE Healthcare) administered every other day. For the long-term drug treatment study, expression of $Nras^{G12D/G12D}$ in LSL $Nras^{G12D/G12D}$ *Mx1-Cre* mice was induced by the leaky expression of *Cre* over time. In all HSC studies, controls were predominantly *Mx1-Cre* mice. In long-term drug treatment studies, controls were either WT C57BL/6 or *Mx1-Cre* mice. In all experiments, control mice were treated exactly the same as $Nras^{G12D/G12D}$ mice (e.g., pI-pC injections), unless otherwise specified.

Flow cytometric analysis of hematopoietic tissues. For lineage analysis of PB, BM, and spleen, flow cytometric analyses were performed as previously described (9). CMPs and CLPs (4, 40) as well as HSCs (41) in BM and spleen were analyzed as previously described. Because hind limb BM represents approximately 25% of total BM (42), the number of HSCs in total BM was calculated as 4 times the number of HSCs in hind limb BM. Stained cells were analyzed on a FACS Calibur or LSRII (BD Biosciences).

Directly conjugated antibodies specific for the following surface antigens were purchased from eBioscience: CD45.2 (clone 104), B220 (clone RA3-6B2), CD19 (clone eBio1D3), Thy1.2 (clone 53-2.1), Mac-1 (clone M1/70), Gr-1 (clone RB6-8C5), CD4 (clone GK1.5), CD8 (clone 53-6.7), CD3 (clone 145-2C11), IgM (clone II/41), IL-7Rα (clone A7R34), Sca1 (clone D7), TER119 (clone TER-119), CD34 (clone RAM34), cKit (clone 2B8). FcγRII/III (clone 2.4G2) was purchased from BD Biosciences. CD150 (clone TC15-12F12.2) was purchased from Biolegend. The following biotin-conjugated antibodies were purchased from eBioscience: B220 (clone RA3-6B2), Gr1 (clone RB6-8C5), CD8 (clone 53-6.7), CD19 (clone eBio1D3), CD4 (clone RM4-5), CD3 (clone 145-2C11), IgM (clone eB121-15F9), IL-7Rα (clone B12-1), TER119 (clone TER-119).

Cell cycle analysis of HSCs. Cell cycle analysis was performed essentially as described previously (11). Cells were stained with PE Cy7–conjugated antibodies against CD41, CD48, B220, TER119, and Gr1 and simultaneously stained for PE-conjugated anti-CD150, APC-conjugated anti-cKit, PerCP Cy5.5–conjugated anti-Sca1, FITC-conjugated anti-Ki67 (BD Biosciences), and DAPI (Invitrogen). Stained cells were analyzed on a LSRII (BD Biosciences).

EdU incorporation in untreated mice. EdU (Invitrogen) was administered as a single dose of 1 mg injected i.p. EdU incorporation in vivo was measured 16 hours later using the Click-It EdU Pacific Blue Flow Kit (Invitrogen) as previously described (24). Stained cells were analyzed on a LSRII (BD Biosciences).

BM transplantation. HSCs were purified as $B220^-Gr1^-TER119^-CD41^-CD48^-Sca1^+cKit^+CD150^+$ BM cells using a FACS AriaII (BD Biosciences) as described previously (24). 20 purified HSCs ($CD45.2^+$) were transplanted with 2×10^5 WBM cells ($CD45.1^+$) into individual lethally irradiated mice as described previously (9).

After long-term treatment with vehicle, AZD6244 alone, AZD1480 alone, or AZD6244 and AZD1480 combined, 5×10^6 WBM cells ($CD45.2^+$) from $Nras^{G12D/G12D}$ mice were transplanted into individual sublethally irradiated mice as described previously (9).

Flow cytometric analysis of pERK1/2, pSTAT5, and pAKT in HSCs and MPPs. Flow cytometric analysis of pERK1/2 and pAKT in HSCs and MPPs were performed as previously described (24, 43). Briefly, $Sca1^+$ cells were enriched from the BM cells using an AutoMACS (Miltenyi Biotec). $CD150^+CD41^-$ (enriched for HSCs) and $CD150^-CD41^-$ cells (enriched for MPPs) were sorted using a FACS AriaII (BD Biosciences). Sorted cells were subjected to phosphoflow analysis. Surface proteins were detected with FITC-conjugated anti-B220 (clone 6B2), anti-Gr1 (clone RB6-8C5), anti-TER119, and anti-CD48 antibodies and PE-conjugated anti-CD117/

cKit antibody (all eBiosciences). pSTAT5 (pY694) was detected by Alexa Fluor 647–conjugated primary antibody against pSTAT5 (BD Biosciences). pERK1/2 and pAKT were detected by primary antibodies against pERK (Thr202/Tyr204; Cell Signaling Technology) and pAKT (Ser473; Cell Signaling Technology), respectively, followed by APC-conjugated donkey anti-rabbit F(ab′)2 fragment (Jackson ImmunoResearch).

Gene expression profiling. 500 HSCs were sorted using a FACS AriaII (BD Biosciences) and used in each biological replica. Sorting purity was routinely >96%. Microarray profiling was performed by Miltenyi Biotech using Agilent Mouse Whole Genome 4X44K array chips. Results were deposited in GEO (accession no. GSE46948). Heat maps were generated using dChip software.

PCR array. 500 HSCs were sorted into RNAprotect Cell Reagent (Qiagen). Total RNAs were extracted using RNEasy Micro Kit (Qiagen). cDNAs were synthesized and amplified using Ovation Pico WTA System V2 (Nugen). Real-time RT-PCR reactions were performed on a CFX96 Real-Time System (Bio-Rad) using the RT² Profiler PCR Array of the Mouse MAPK Pathway (SABiosiences/Qiagen) according to the manufacturer's instructions.

Single HSC genotyping. Single HSCs were sorted into 96-well plates containing M3434 medium (StemCell Technologies) supplemented with 10 ng/ml murine GM-CSF and TPO (Pepro Tech), then cultured in vitro at 37°C for 14 days. Genomic DNA was extracted from Methocult colonies using a HotSHOT method (44).

Flow cytometric analysis of pERK1/2, pSTAT5, and pAKT in progenitor cells. Total BM cells were serum and cytokine starved for 90 minutes and incubated with vehicle, AZD6244 alone, AZD1480 alone, or AZD6244 and AZD1480 combined for another 30 minutes at 37°C. Cells were then stimulated with 10 ng/ml GM-CSF or SCF for 10 minutes at 37°C. pERK1/2, pSTAT5, and pAKT were analyzed in defined $Lin^{-/lo}cKit^{+}$ cells essentially as previously described (4).

Cell culture. JMML/MP-CMML cells from $Nras^{G12D/G12D}$, $Nras^{G12D/+}$, and $Kras^{G12D/+}$ mice or CMML patient cells were cultured in SFEM (StemCell Technologies) with 10% FBS plus 0.2 ng/ml murine or human GM-CSF, respectively (Pepro Tech). Cells were seeded at 2×10^5/ml in triplicate in 96-well plates in the presence of DMSO or various concentrations of AZD6244 and/or AZD1480. After 5, 7 ($Nras^{G12D/G12D}$, $Nras^{G12D/+}$, and $Kras^{G12D/+}$ cells), or 14 days (human CMML cells) in culture, cell viability was determined using the CellTiter Glo Assay (Promega) according to the manufacturer's instructions.

Complete blood count and histopathology. Complete blood count analysis was performed using a Hemavet 950FS (Drew Scientific). Mouse tissues were fixed in 10% neutral buffered formalin (Sigma-Aldrich) and further processed at the UWCCC Histology Lab.

Administration of small compounds in $Nras^{G12D/G12D}$ mice. AZD6244 and AZD1480 (Sequocia and ChemieTek) were resuspended in water supplemented with 0.5% hypromellose and 0.1% Tween 80 and administered by oral gavage twice daily as described previously (29–31, 45). For short-term treatment with AZD6244 alone (50 mg/kg), AZD1480 alone (12.5 mg/kg), or AZD6244 (25 mg/kg) and AZD1480 (12.5 mg/kg) combined, treatment started 2 days after the last pI-pC injection and lasted for 7 days. For long-term treatment with AZD6244 alone (25 or 50 mg/kg), AZD1480 alone (12.5 mg/kg), or AZD6244 (25 mg/kg) and AZD1480 (12.5 mg/kg) combined, treatment started when the wbc count in PB exceeded 40×10^3 and lasted for 20 weeks or until mice became moribund. Rapamycin (LC Laboratories) was administered at 4 mg/kg daily by i.p. injection as described previously (25). The injection scheme was the same as that for AZD6244 short-term treatment.

Statistics. Kaplan-Meier survival analysis was performed, and survival differences between groups were assessed with the log-rank test. Unpaired 2-tailed Student's *t* tests were used to determine the significance between 2 data sets. A *P* value less than 0.05 was considered significant.

Study approval. All animal experiments were conducted in accordance with the NIH *Guide for the Care and Use of Laboratory Animals* and approved by an Animal Care and Use Committee at University of Wisconsin-Madison. The program is accredited by the Association for Assessment and Accreditation of Laboratory Animal Care. Primary human CMML samples were obtained from the UWCCC TSB Biobank with institutional review board approval. Patient consent was waived.

Acknowledgments

The authors thank Emery Bresnick and Qiang Chang for helpful discussion and critical comments on the manuscript as well as UWCCC for use of its Shared Services to complete this research. This work was supported by R01 grants 1R01CA152108 and 1R01HL113066, a Shaw Scientist Award from the Greater Milwaukee Foundation, a Scholar Award from the Leukemia and Lymphoma Society, and an Investigator Initiated Grant from UWCCC to J. Zhang. This work was also supported in part by NIH/NCI P30 CA014520 — UW Comprehensive Cancer Center Support, an Institutional Clinical and Translational Science Award (NIH/NCRR grant 1UL1RR026314-01), a Translational Trials Development and Support Laboratory award (USPHS grant MO1 RR08084), and a Center of Excellence in Molecular Hematology P30 award (DK090971). J.C. Mulloy is a Leukemia and Lymphoma Society Scholar. We dedicate this work to Eric McLean, who fought bravely with AML for 9 years and passed away in August 2012. The Leukemia Ironman Fundraiser For Eric, a nonprofit organization founded by his family, provided initial financial support for this project.

Received for publication November 7, 2013, and accepted in revised form March 20, 2014.

Address correspondence to: Jing Zhang, Room 417A, McArdle Lab, 1400 University Avenue, University of Wisconsin-Madison, Madison, Wisconsin 53706, USA. Phone: 608.263.1147; Fax: 608.262.2824; E-mail: zhang@oncology.wisc.edu.

1. Emanuel PD. Juvenile myelomonocytic leukemia and chronic myelomonocytic leukemia. *Leukemia*. 2008;22(7):1335–1342.
2. Dunbar AJ, et al. 250K single nucleotide polymorphism array karyotyping identifies acquired uniparental disomy and homozygous mutations, including novel missense substitutions of c-Cbl, in myeloid malignancies. *Cancer Res*. 2008; 68(24):10349–10357.
3. Kohlmann A, et al. Next-generation sequencing technology reveals a characteristic pattern of molecular mutations in 72.8% of chronic myelomonocytic leukemia by detecting frequent alterations in TET2, CBL, RAS, and RUNX1. *J Clin Oncol*. 2010;28(24):3858–3865.
4. Wang JY, et al. Endogenous oncogenic Nras mutation leads to aberrant GM-CSF signaling in granulocytic/monocytic precursors in a murine model of chronic myelomonocytic leukemia. *Blood*. 2010;116(26):5991–6002.
5. Kato M, et al. Aggressive transformation of juvenile myelomonocytic leukemia associated with duplication of oncogenic KRAS due to acquired uniparental disomy. *J Pediatr*. 2013;162(6):1285–1288.
6. Ward AF, Braun BS, Shannon KM. Targeting oncogenic Ras signaling in hematologic malignancies. *Blood*. 2012;120(17):3397–3406.
7. Braun BS, et al. Somatic activation of oncogenic Kras in hematopoietic cells initiates a rapidly fatal myeloproliferative disorder. *Proc Natl Acad Sci U S A*. 2004;101(2):597–602.
8. Chan IT, et al. Conditional expression of oncogenic K-ras from its endogenous promoter induces a myeloproliferative disease. *J Clin Invest*. 2004;113(4):528–538.
9. Zhang J, et al. Oncogenic Kras-induced leukemogeneis: hematopoietic stem cells as the initial target and lineage-specific progenitors as the potential targets for final leukemic transformation. *Blood*. 2009;113(6):1304–1314.
10. Li Q, et al. Hematopoiesis and leukemogenesis in mice expressing oncogenic NrasG12D from the endogenous locus. *Blood*. 2011;117(6):2022–2032.
11. Wang JY, et al. Endogenous oncogenic Nras mutation initiates hematopoietic malignancies in a dose- and cell type-dependent manner. *Blood*. 2011;118(2):368–379.
12. Wang J, et al. Distinct requirements of hematopoi-

etic stem cell activity and Nras G12D signaling in different cell types during leukemogenesis. *Cell Cycle*. 2011;10(17):2836–2839.
13. Du J, et al. Loss of CD44 attenuates aberrant GM-CSF signaling in Kras G12D hematopoietic progenitor/precursor cells and prolongs the survival of diseased animals. *Leukemia*. 2013;27(3):754–757.
14. Lyubynska N, et al. A MEK inhibitor abrogates myeloproliferative disease in Kras mutant mice. *Sci Transl Med*. 2011;3(76):76ra27.
15. Chang T, et al. Sustained MEK inhibition abrogates myeloproliferative disease in Nf1 mutant mice. *J Clin Invest*. 2013;123(1):335–339.
16. Flaherty KT, Hodi FS, Bastian BC. Mutation-driven drug development in melanoma. *Curr Opin Oncol*. 2010;22(3):178–183.
17. Lauchle JO, et al. Response and resistance to MEK inhibition in leukaemias initiated by hyperactive Ras. *Nature*. 2009;461(7262):411–414.
18. Jessen WJ, et al. MEK inhibition exhibits efficacy in human and mouse neurofibromatosis tumors. *J Clin Invest*. 2013;123(1):340–347.
19. Emery CM, et al. MEK1 mutations confer resistance to MEK and B-RAF inhibition. *Proc Natl Acad Sci U S A*. 2009;106(48):20411–20416.
20. Hatzivassiliou G, et al. ERK inhibition overcomes acquired resistance to MEK inhibitors. *Mol Cancer Ther*. 2012;11(5):1143–1154.
21. Sabnis AJ, et al. Oncogenic Kras initiates leukemia in hematopoietic stem cells. *PLoS Biol*. 2009; 7(3):e59.
22. Van Meter ME, et al. K-RasG12D expression induces hyperproliferation and aberrant signaling in primary hematopoietic stem/progenitor cells. *Blood*. 2007;109(9):3945–3952.
23. Kotecha N, et al. Single-cell profiling identifies aberrant STAT5 activation in myeloid malignancies with specific clinical and biologic correlates. *Cancer Cell*. 2008;14(4):335–343.
24. Wang J, et al. Nras G12D/+ promotes leukemogenesis by aberrantly regulating haematopoietic stem cell functions. *Blood*. 2013;121(26):5203–5207.
25. Yilmaz OH, et al. Pten dependence distinguishes haematopoietic stem cells from leukaemia-initiating cells. *Nature*. 2006;441(7092):475–482.
26. Orford KW, Scadden DT. Deconstructing stem cell self-renewal: genetic insights into cell-cycle regulation. *Nat Rev Genet*. 2008;9(2):115–128.
27. Krivtsov AV, et al. Transformation from committed progenitor to leukaemia stem cell initiated by MLL-AF9. *Nature*. 2006;442(7104):818–822.
28. Serrano M, Lin AW, McCurrach ME, Beach D, Lowe SW. Oncogenic ras provokes premature cell senescence associated with accumulation of p53 and p16INK4a. *Cell*. 1997;88(5):593–602.
29. Yeh TC, et al. Biological characterization of ARRY-142886 (AZD6244), a potent, highly selective mitogen-activated protein kinase kinase 1/2 inhibitor. *Clin Cancer Res*. 2007;13(5):1576–1583.
30. Davies BR, et al. AZD6244 (ARRY-142886), a potent inhibitor of mitogen-activated protein kinase/extracellular signal-regulated kinase kinase 1/2 kinases: mechanism of action in vivo, pharmacokinetic/pharmacodynamic relationship, and potential for combination in preclinical models. *Mol Cancer Ther*. 2007;6(8):2209–2219.
31. Hedvat M, et al. The JAK2 inhibitor AZD1480 potently blocks Stat3 signaling and oncogenesis in solid tumors. *Cancer Cell*. 2009;16(6):487–497.
32. Wunderlich M, et al. AML xenograft efficiency is significantly improved in NOD/SCID-IL2RG mice constitutively expressing human SCF, GM-CSF and IL-3. *Leukemia*. 2010;24(10):1785–1788.
33. Li Q, et al. Oncogenic Nras has bimodal effects on stem cells that sustainably increase competitiveness. *Nature*. 2013;504(7478):143–147.
34. Tuveson DA, et al. Endogenous oncogenic K-ras(G12D) stimulates proliferation and widespread neoplastic and developmental defects. *Cancer Cell*. 2004;5(4):375–387.
35. Burdon T, Stracey C, Chambers I, Nichols J, Smith A. Suppression of SHP-2 and ERK signalling promotes self-renewal of mouse embryonic stem cells. *Dev Biol*. 1999;210(1):30–43.
36. Vaudry D, Stork PJ, Lazarovici P, Eiden LE. Signaling pathways for PC12 cell differentiation: making the right connections. *Science*. 2002; 296(5573):1648–1649.
37. Zhang J, Lodish HF. Constitutive activation of the MEK/ERK pathway mediates all effects of oncogenic H-ras expression in primary erythroid progenitors. *Blood*. 2004;104(6):1679–1687.
38. Reynaud D, et al. IL-6 controls leukemic multipotent progenitor cell fate and contributes to chronic myelogenous leukemia development. *Cancer Cell*. 2011;20(5):661–673.
39. Wang Y, et al. Mutant N-RAS protects colorectal cancer cells from stress-induced apoptosis and contributes to cancer development and progression. *Cancer Discov*. 2013;3(3):294–307.
40. Kondo M, Weissman IL, Akashi K. Identification of clonogenic common lymphoid progenitors in mouse bone marrow. *Cell*. 1997;91(5):661–672.
41. Kiel MJ, et al. Haematopoietic stem cells do not asymmetrically segregate chromosomes or retain BrdU. *Nature*. 2007;449(7159):238–242.
42. Boggs DR. The total marrow mass of the mouse: a simplified method of measurement. *Am J Hematol*. 1984;16(3):277–286.
43. Du J, et al. Signaling profiling at the single cell level identifies a distinct signaling signature in murine hematopoietic stem cells. *Stem Cells*. 2012; 30(7):1447–1454.
44. Truett GE, Heeger P, Mynatt RL, Truett AA, Walker JA, Warman ML. Preparation of PCR-quality mouse genomic DNA with hot sodium hydroxide and tris (HotSHOT). *Biotechniques*. 2000;29(1):52.
45. Xin H, et al. Antiangiogenic and antimetastatic activity of JAK inhibitor AZD1480. *Cancer Res*. 2011; 71(21):6601–6610.